Physical response of the tropical-subtropical North Atlantic Ocean to decadal-multidecadal forcing by African dust

Amato T. Evan[1,*], Gregory Foltz[2], Dongxiao Zhang[3]

[1]University of Virginia, Department of Environmental Sciences, Charlottesville, Virginia

[2]Atlantic Oceanographic and Meteorological Laboratory (NOAA/AOML), Miami, Florida

[3]Pacific Marine Environmental Laboratory (NOAA/PMEL), Seattle, Washington

*To whom correspondence may be addressed: aevan@virginia.edu

To be submitted: *Journal of Climate* Abstract

Dust storms are a persistent feature over the tropical North Atlantic which vary in magnitude over a wide range of time scales. While it is well known that mineral aerosols alter radiative fluxes from the surface through the top of the atmosphere, much less is understood about the oceanic response to such change in radiation, particularly on long time scales. In this study we use an observation-based climatology of dust surface forcing and an ocean general circulation model to explore the effect of anomalous dust over the tropical North Atlantic during the period 1955–2008. Our findings demonstrate that variability in dust forces decadal-scale variability of temperatures at the sea surface and below the mixed layer, which are of magnitude comparable to observed variability. On longer time scales dust forced sea surface temperature anomalies vary in phase with the Atlantic Multidecadal Oscillation, suggesting that tropical North Atlantic multidecadal variability is to some extent externally forced by dust. Up to now estimates of the magnitude of the response of the ocean to dust variability on interannual to multidecadal time scales have been made with coupled general circulation models, thus these results provide an independent data set for comparison and evaluation of such coupled numerical experiments.

1. Introduction

Dust outbreaks from West Africa are a persistent feature of the tropical North Atlantic (*Kaufman et al.* 2005) and estimates of annual emissions of dust range from 170 to 1600 Tg (*Engelstaedter et al.* 2006), although models may underestimate the actual emissions (*Kok* 2011). Mineral aerosols have a high single scatter albedo (*Myhre et al.* 2003) and over dark surfaces net effect of dust is to displace radiation at the surface to the height of the dust layer (*Wong et al.* 2009) or the top of the atmosphere (*Evan and Mukhopadhyay* 2010).Therefore, by bulk formulae, the presence of an elevated aerosol layer over water would tend to cool the ocean.

Schollaert and Merril (1998) showed a negative correlation between individual dust outbreaks and underlying SST, and used a mixed-layer heat budget analysis to suggest that the magnitude of the aerosol direct effect was sufficiently large to force the observed cool anomalies. *Evan et al.* (2008) demonstrated that on longer time scales such a statistical relationship held, showing that the cross-correlation function of monthly mean SST and dust optical depth anomalies is a maximum when SST lagged the dust by one to three months. *Foltz and McPhadden* (2008a) used *in-situ* data from tropical North Atlantic moorings, and a mixed-layer heat budget analysis, to suggest that 35% of the historical (1984–2000) year-to-year changes in summertime SST was radiatively forced by dust. *Evan et al.* (2008) suggested that a secular downward trend in dust optical depth, from the early 1980s through the early 2000s may have contributed to the upward trend in tropical North Atlantic SST over this same period. *Foltz and McPhadden* (2008b) used an independent satellite data set to show that the downward trend in dust, if left

unbalanced by other processes, would lead to an increase in 3° C of the tropical North Atlantic mixed layer. *Evan et al.* (2009) used a 1-D mixed layer model and a highly idealized parameterization of ocean-atmosphere heat fluxes to show that this trend in dust contributed to 20% of observed upward SST trend, averaged over the region. Lastly, *Martinez Avellaneda* (2010) used microwave retrieved SST to show that from 2000-2006 approximately 30% of SST variability in the eastern tropical-subtropical North Atlantic, with individual outbreaks cooling SST by 0.2°-0.4° C. They also show that in an ocean general circulation model, the climatological SST cooling by dust is approximately 0.5°C.

These empirically-based studies all consistent that dust plays an important role in shaping the observed variability of tropical North Atlantic SST. However, results from general circulation model experiments differ in terms the influence of dust on SST, ranging from virtually no effect (*Miller and Tegen*, 1998) to mean cooling *O*(0.5° C) (*Yoshioka et al.* 2008), where discrepancies are likely related to dust mass fluxes and aerosol radiative properties (*Huneeus et al.* 2010). Most recently, *Mahowald et al*. (2010), employing an atmospheric general circulation model coupled to a slab ocean, showed an annually-averaged dust-forced change in SST between two 10-year periods of high and low dust concentrations (1955-1964 and 1980-1989), with cooler SST during the period of elevated dust between 0.1°-0.5°C, over the tropical North Atlantic.

Given the current state of understanding regarding aeolian dust and tropical North Atlantic SST several important questions remain unanswered related to the role of these mineral aerosols and regional climate. Principally among them, what is the influence of dust on regional SST on decadal to multidecadal time scales? Elucidating such physical

processes on decadal time scales is the focus of this study. The remainder of this manuscript is organized as follows: In Section 2 we discuss the physical ocean model used here, including discussion of the dust surface forcing climatology, and a validation of the model setup. In Section 3 we examine the output of our numerical experiments, focusing on temperature variability of the surface and subsurface, but also considering heat content and velocity anomalies of the upper ocean. We conclude in Section 4 with discussion of the results in the context of understanding climate of the tropical North Atlantic.

2. Data and Models

In this manuscript we examine the physical response of the upper ocean to variability in aeolian dust on interannual to decadal time scales using a long-term climatology of Atlantic dust radiative forcing at the surface and an ocean general circulation model. The following is a brief discussion of the dust climatology, which is described in more detail in *Evan and Mukhopadhyay* (2010), and an more thorough description of the numerical ocean model employed here.

a. Atlantic dust climatology

Historical (1955–2008), monthly mean dust surface radiative forcing estimates, at a 1° horizontal resolution, are from *Evan and Mukhopadhyay* (2010), and we refer the reader to this paper for an in-depth discussion of the data set. Briefly, this climatology employs a mixture of satellite and *in-situ* proxy data to generate monthly maps of dust optical depth over the northern tropical Atlantic. When compared to satellite observations for the period of 1982–2008 the dust climatology explains 68% of the monthly mean dust optical depth over the tropical North Atlantic (10W-65W, 0N-30N). Surface radiative

forcing is then estimated from the optical depth values using a radiative transfer model. One limitation of this climatology is that at any location in tropical Atlantic annual mean dust optical depth and surface forcing is perfectly correlated with dust optical depth at Cape Verde, due to the regression model used in the reconstruction, although the means and standard deviations do not necessarily equate. However, this is not the case for the monthly dust optical depth and radiative forcing values, which are inversely proportional to total cloud cover.

From this climatology, long-term mean Atlantic dust cover extends westward from the coast of West Africa to the Caribbean, and spans the latitudes of 5°-25°N, with the highest concentrations between 15°-45°W and 10°-20°N (Fig. 1). Dust in the northern tropical Atlantic exhibits a pronounced seasonal cycle; there is a minimum during the November-December period and a maximum during June-July. The summertime maximum in dust loading is more than three times the wintertime minimum value (Fig. 2), consistent with satellite estimates of the dust seasonal cycle (Husar et al. 1997; Kaufman et al. 2005). From 1955–2008 annual mean dust optical depth averaged over the northern tropical Atlantic (Fig 2), is characterized by a peak in dustiness during the mid-1980s, consistent with *Prospero and Lamb* (2003), and minima in dust cover during the mid-1950s and mid-1960s, consistent with *Mahowald et al.* (2010), and during the 2000s, consistent with *Evan et al.* (2009).

Dust direct surface radiative forcing closely follows optical depth variability; there is a maximum in the magnitude of the surface forcing in July, and a minimum during the boreal fall and winter seasons (*Evan and Mukhopadhyay* 2010). The range of annual mean surface direct forcing averaged over the northern tropical Atlantic is -5 to -6

Wm^{-2}, and monthly mean values range from -3 to -9 Wm^{-2}. The maximums and minimums in the magnitude of the forcing occur simultaneously with the maximums and minimums in dust optical depth.

b. Ocean general circulation model

We use the Massachusetts Institute of Technology Ocean General Circulation Model (MITgcm) (*Marshall et al.* 1997a; *Marshall et al.* 1997b) to estimate the physical response of the ocean to dust forcing. The MITgcm is run globally with a horizontal resolution of 1° and 23 vertical layers, with the uppermost layers having a resolution of 10 m and the lower layers becoming coarser with depth to a maximum of 500 m. The bathymetry extends from 80°S to 80°N. The Gent-McWilliams (*Gent and McWilliams* 1990) eddy parameterization and KPP vertical mixing scheme (*Large et al.* 1994) simulate effects of sub-grid-scale processes. Surface temperature and salinity are relaxed to a monthly climatology from the World Ocean Atlas (*Boyer et al.* 2005) at time scales of two and six months, respectively. Model tracers and momentum have a time step of 240s.

For model spin up we use climatological monthly surface horizontal momentum fluxes from the National Centers for Environmental Protection (NCEP) Reanalysis I (*Kalnay et al.* 1996) and climatological monthly surface heat budgets that are calculated offline using NCEP Reanalysis 1 surface fluxes of long and shortwave radiation and sensible and latent heat. The model is spun up to steady state in the upper ocean for 100 years using a momentum time step of 240 s and a tracer time step of 6 hrs. The model is run for an additional 30 years with momentum and tracer time steps set to 240 s.

For the model spinup and the numerical experiments surface relaxation to observed salinity and temperature is required to reproduce observed SST and surface salinity in the model. Also, model SST relaxation is analogous to a parameterization of the turbulent fluxes of latent and sensible heat that act to dampen an SST anomaly (e.g., *Deser et al.* 2003; *Evan et al.* 2009). SST relaxation in the context of dampening of SST anomalies is examined below by considering changes in SST due to radiative forcing by stratospheric aerosols from two major volcanic eruptions. SST relaxation is achieved by modifying the surface heat budget in order to linearly relax the model SST to the prescribed values over the designated relaxation time, i.e.,

Eqn. 1

where H_{flux} is the original surface heat flux, ρ is the density and c_p is the specific heat of seawater, Δh is the depth of the first model level (10 m), SST_{model} is the model output SST, SST_{relax} is the prescribed SST that the model is relaxed to, t_{relax} is the chosen relaxation time, and H^*_{flux} is the new surface heat flux required to satisfy (1). Suspended dust cools local SSTs mostly via reductions in downwelling SW radiation (*Evan et al.* 2009), so that dust-forced changes to H_{flux} are damped according to t_{relax}. Thus, the magnitude of the response of the upper ocean to dust is sensitive to the choice of t_{relax}.

We compare the state of the physical model after the 130 year spinup with a t_{relax} of two weeks and two months. For the model data we consider long term mean SST to be the annually averaged SST from the final year of the 130 year spinup run. We compare the model SST to long-term annual mean SST the WOA05 data set; which is the SST climatology which we relax model SST to. Model SST for t_{relax} of two months shows regions of disagreement with the observations that can be characterized as cool anomalies

along the western boundary currents, and anomalously warm temperatures over the Guinea Dome and subtropical northern and southern regions (Fig 3). Disagreement between the model and observations is less than $2°C$ over much of the basin, although larger values are seen in the Caribbean, Gulf Stream, and the Guinea Dome close the the coast of West Africa. By definition, model SST output with t_{relax} two weeks shows better agreement to the observations over the tropical and subtropical Atlantic. While the same broad pattern of anomalously warm SST to the east and cool SST to the west holds, differences between the two data are $O(1°C)$ or less (Fig 3). Over much of the basin the use of the shorter t_{relax} period reduces disagreement between the model and observations by approximately 50%.

We also consider differences in the seasonal cycle between the model output and climatological monthly mean SST observations by examining the differences between mean summer (JAS) and winter (FMA) SST (Fig 4). Model output for both t_{relax} values underestimates the magnitude of the seasonal cycle south of the equator and overestimates it north of 30°N, but the disagreement is roughly $1°C$ greater in magnitude for the longer relaxation time. Over much of the northern tropical Atlantic, our region of interest, the modeled annual cycle better agrees with observations, and the differences between the model and observations for each model configuration are $O(\ 1°C)$ or less.

From the comparisons of modeled and observed, and by definition, SST t_{relax} of two weeks will produce more realistic model surface temperatures (Figs 3–4). However, the shorter relaxation time will also more strongly damp dust-forced SST anomalies and may cause the model to underestimate the impact of the aerosol direct effect on surface temperatures.

We examine the sensitivity of model SST anomalies that are forced by perturbations to the surface heat flux to the value of t_{relax} by examining the change in SST that followed the eruptions of El Chichón in 1982, and Mount Pinatubo in 1991. After each of these major eruptions elevated levels of stratospheric aerosols greatly reduced the surface solar insolation, thus cooling surface and subsurface temperatures globally. The SST response to each eruption is unique to other forms of internally and externally forced variability and therefore it is possible to isolate the volcanic signal in observed SST. To do so we create a monthly time series of observed SST (*Rayner et al.* 2002) for the time period of 1980-2000 that is averaged over the northern tropical Atlantic (0°-30°N and 20°-65°W). The observed SST time series is de-seasonalized by subtracting from every monthly mean SST value the climatological mean of that month, and de-trended to remove variability associated with greenhouse gas forcing or other secular processes. In order to quantify the magnitude of the aerosol-forced changes in the observed SST time series, the SST anomalies must be defined as relative to an average SST over some base period. Following the methodology of *Santer et al.* (1995), we define anomalies relative to the mean SST for the one, two, and three years preceding the 1982 eruption of El Chichón (however the anomalies are similar for the shorter periods). The resulting SST anomaly time series exhibits cool anomalies on the order of 0.5°C in the year following the eruptions of El Chichón and Mount Pinatubo (Fig. 5) consistent with other studies (*Evan et al.* 2009; *Santer et al.* 1995).

We next model the response of SSTs to these eruptions for t_{relax} values of two weeks, one month, and two months. SST forcing by stratospheric aerosols is determined by differencing the output of a control run from a perturbation run. The control run is

forced by seasonally varying reanalysis surface heat fluxes and horizontal wind stress for 23 years. The perturbation run is forced by the same seasonally varying surface fluxes of heat and momentum, but the heat flux is modified to account for changes in downwelling radaiative fluxes due to the buildup and decay of stratospheric aerosols. Estimates of the volcanic aerosol radiative forcing at the surface is from *Evan et al.* (2009). The difference of SST from the two model runs is interpreted as the effect of volcanic eruptions on tropical North Atlantic SST (Fig 5).

The sensitivity of model SST to the eruptions grows progressively larger as t_{relax} varies from two weeks to two months (Fig. 5). Model SST anomalies appear to underestimate the influence of stratospheric aerosols for t_{relax} of two weeks, evidenced by a maximum anomaly of magnitude less than 0.2°C after each eruption, nearly one-third of the observed cooling. Model SST anomalies for t_{relax} of one month are closer to the large peak in cooling that follows each eruption, but still are only able to reproduce half of the observed cooling. Model SST anomalies for t_{relax} of two months appear to well represent the dramatic cooling observed in the one to two years following each eruption, but may still underestimate this cooling by 0.1°C. The progressively weaker response of SST to aerosol forcing as the relaxation time scale becomes shorter can be interpreted as analogous to reducing the time scale over which SST anomalies are damped to the atmosphere by turbulent fluxes of latent and sensible heat.

Although model t_{relax} of two months is less effective at reproducing climatological SST (Figs 3, 4), a t_{relax} of two weeks to one month underestimates the effect of radiatively forced SST anomalies and presumably temperature anomalies at depth (Fig 5). We therefore use a relaxation timescale of two months for this study. These results imply that

completely turning off SST relaxation in the model may lead to an overestimation of dust radiatively forced SST anomalies (*Avellende et al.* 2010). We note that a relaxation time scale of two months is similar to the dampening time scale used by *Evan et al.* (2009).

Lastly, modeled annual mean upper ocean currents, averaged over the top 100 *m* of the ocean, with t_{relax} of two months, appear to capture the western boundary currents of the tropical and subtropical Atlantic (Fig 6). The model layer thicknesses in the top *100 m* are, from the surface down, 10, 10, 15, 20, 20, and 25 *m*. The model produces a North Brazil Current (NBC), including retroflection of the NBC just north of the equator to feed the Northern Equatorial Counter Current (NECC), as well as the Guiana, Antilles, and Florida Currents, and Gulf Stream. Also apparent are the Caribbean Current and Gulf Loop Current, which are fed from the NBC and in-turn feed the Florida Current. To the east are visible eastern branches of the northern Subtropical Gyre, including the southwestward Azores and Canary Currents. Closer to the equator the model also reproduces the westward North and South Equatorial Currents (NEC and SEC, respectively), and the eastward NECC. The modeled western boundary currents are wider than in real ocean, a typical limitation in coarse resolution models.

Surface winds and heat flux data from other available reanalysis may better reproduce observed climatological SST with this long relaxation time. Additionally, adding to the NCEP reanalysis heat fluxes the H^{*}_{flux} (Eqn 1) output from spinup model runs where t_{relax} is equal to two weeks, prior to running the experiments with t_{relax} set to two months, may improve the reproduction of climatological SST. Both options will be explored in future studies. However, given that this analysis involves differencing the

output from two very similar model runs, we anticipate that such improvement in the model mean state will have a negligible effect on the results presented here.

3. Numerical experiment results

As previously stated we use the dust surface forcing climatology of *Evan and Mukhopadhyay* (2010) to estimate the physical response of the ocean to dust variability over time. We perform a model control and perturbation run, each initialized from the 130 year spinup that was described in Section 2, similar to the experiments used to estimate the effect of volcanic eruptions on SST (Fig 5). In the control run we integrate forward from the spinup run an additional 54-years (1955–2008) using the same seasonally varying monthly surface forcing. For the perturbation run we subtract from the seasonal surface heat fluxes the contribution from radiative forcing by anomalous dust variability. The dust contribution to the surface heat flux is defined as the dust aerosol direct effect at the surface minus the long term mean, and minus the dust forcing annual cycle, which is removed by subtracting from each monthly forcing value the long term mean of that month. We remove the long-term mean and the seasonal variability from the dust forcing climatology because we are assuming that climatological monthly surface heat fluxes from reanalysis already reflect the mean forcing from dust. Although such an assumption is not justified by observations, it is more conservative that not removing the long-term and seasonal mean from the dust forcing climatology, since the dust-forced perturbations we use here are on the order of 1-2 Wm^{-2}, which is much smaller than 5-15 Wm^{-2} forcing in the raw climatology (*Evan and Mukhopadhyay*, 2010). We interpret the difference of the control from the perturbation run to be the effect of departures in

dustiness from the seasonal mean state on the state of the ocean. We note that since we force the model with the climatological seasonal cycle of reanalysis heat fluxes instead of fluxes that also vary from year-to-year, we are in-effect estimating the influence of dust variability about the mean state of the ocean.

a. Sensitivity of SST to dust variability

As we are modeling the effect of departures in dustiness from the seasonal mean the long term mean dust-forced change in SST (hereafter referred to as ΔSST) is everywhere $O(0.001°C)$. In order to provide insight into the spatial pattern of ΔSST we examine the range of ΔSST values over the northern tropical Atlantic (Fig. 7), which we interpret to indicate the spatial pattern of the sensitivity of the ocean to historical dust variability. The maximum range of ΔSST is greater than 0.7°C and centered on the region of 20°-30°W and 15-25°N, matching the maximum in climatological dust optical depths (Fig 1). The area of maximum (in magnitude) climatological dust surface radiative forcing is to the east of ΔSST, reflecting the influence of the cloud field in modifying the direct effect, the structure of the ocean mixed layer (Evan et al. 2009), and other internal processes that govern the oceanic response to the modification of the surface heat flux (Fig 7).

We note that the 0.1°C ΔSST contour is very similar in shape to the 2 W m^{-2} all-sky forcing contour, suggesting that further west the SST response to dust is largely the result of changes to the surface heat budget by dust rather than by dynamic advection. To the west the gradient of ΔSST is weaker than to the north or south, coincident with

structure of the climatological dust optical depth (Fig 1), and the southern branch of the subtropical Gyre, or the NEC (Fig 6).

b. SST time series analysis

From 1955–2008 monthly mean ΔSST, averaged over 12.5°-25°N and 20°-60°W (black box, Figs 3-4), has a range of 0.43°C with coherent 10 to 20 year periods of warm and cool anomalies (Fig. 8). A 5-year low pass filtered annual mean time series of ΔSST (achieved using two recursive 3-year running mean filters) highlights these anomalous coherent periods, including: warm anomalies from the beginning of the record to 1970, a cool period from 1970 through 1976 that is followed by a brief warm anomaly of three years, a 15 year cool anomaly from 1979 through 1994, and then a 14 year warm anomaly from 1995 through the end of the record.

Warming from anomalously low dust cover during the late 1950s and cooling from the more intense and persistent dust cover during the 1980s was noted by Mahowald et al. (2010) although the magnitude and spatial pattern of ΔSST in the Mahowald et al. study do not appear to corroborate these results. Additionally, the cool period during the 1980s and the transition from a minimum around 1985 to a maximum in the mid 2000s have been noted by Evan et al. (2009) and Foltz and McPhaden (2008).

Over this same region 5-year low pass filtered observed SST anomalies have a range of 1.0°C and also show coherent periods of cool and warm anomalies (Fig. 8) that are both internally and externally forced (*Trenberth and Shea* 2006; *Evan et al.* 2009). The observed period of cool and warm SST anomalies seemingly match the anomalous periods of ΔSST. For example, there are warm anomalies in each time series from 1995

onward, and both show the magnitude of this anomaly being near zero during 2000. Likewise, observed warm SST anomalies from 1995 through 1970 tend to match those in the *ΔSST* series. The observed cool anomaly from 1982–1995 is preceded by the cool dust-forced anomaly starting in 1979. This coherence in anomalies between the two suggests that either changes in dust cover are forced by the same processes that are governing SST variability (*Wong et al.* 2008), or that changes in SST are simultaneously affecting African rainfall and thus dustiness (*Prospero and Lamb* 2003, *Giannini et al.* 2003, *Foltz and McPhaden* 2008).

The *ΔSST* series also shows possible multidecadal-scale variability, with mostly warm anomalies from 1955-1970 (15 years), cool anomalies from 1970-1995 (25 years), and again warm anomalies from 1995-2008 (13 years, Fig 9). Although there is clearly not enough data to detect a robust multidecadal signal in SST that is forced by dust, the results do indicate that any such oscillation would have a period *O*(50 years) and an amplitude *O*(0.1°C). The dust-forced SST variability during 1955-2008 is in phase with the Atlantic multidecadal oscillation (AMO; *Goldenberg et al.* 2001) and about half the amplitude (Fig 9), further suggesting the possibility of positive coupled feedbacks between SST, Sahel rainfall, and African dust on multidecadal timescales.

We examine decadal-scale variability of *ΔSST* by subtracting from the 5-year smoothed annual time series (Fig 8) two recursive 17-year running mean filters that include the series endpoints, this is qualitatively similar to removing the downward linear trend in the data from the beginning of the series to the peak in the cool anomaly (1985), and the upward linear trend from 1985 through 2008. A longer time series for which a

more formal analysis of decadal-scale variability could be evaluated for significance would warrant more careful smoothing, but for our illustrative purposes this approach is acceptable.

Except for the anomalous cool period that persists from 1980–1990, the band-pass filtered time series of ΔSST exhibits regular decadal-scale variability with an amplitude of 0.05°C (Fig 10), which is one-half the magnitude of the five-year smoothed ΔSST anomalies (Fig 8). Cool anomalies are observed during the first-half and warm anomalies are observed during the second-half of each decade (Fig 10). A Fourier Transform of the band pass filtered ΔSST shows spectral peaks that are greater in magnitude than a red noise spectrum (based on the 1-lag autocorrelation of the filtered ΔSST series) at periods of 7–13 years (Fig 10). We note that due to the short length of the ΔSST it is not possible to accurately determine how robust the decadal signal is. However, our results do support development and analysis of longer dust proxy records that are resolved at the annual scale to further elucidate such decadal effects.

c. Spatial structure of dust forced changes to SST, velocity, and heat content

Having considered changes in dust-forced SST anomalies averaged over a subset of the tropical North Atlantic during 1955–2008, we next examine the spatial structure of the upper ocean response to dust variability and consider the governing physical processes. As previously discussed we model the effect of anomalous dust surface forcing, and therefore the long term mean of the perturbation model run is nearly equal to the long term mean of the control run, and at the surface these differences are everywhere $O(0.001°C)$. To examine the spatial structure of the effect of anomalous dustiness on the

upper ocean we instead quantify the effect of dust variability on the state of the upper ocean by differencing composites of the five years for which annually averaged *ΔSST* (Fig 10) was the most negative (1983–1988) and the most positive (1956–1958, 2004, 2005).

The composite difference map of *ΔSST* (Fig 11) is similar in structure to the range of monthly *ΔSST* anomalies (Fig 7), and the maximum magnitude of the SST difference is slightly less than 0.4°C, compared to nearly 0.8°C for the total *ΔSST* range. The -0.05°C contour extends to the eastern Caribbean, and is meridionally bound by the equator and 32°N latitude. While the *ΔSST* composite closely follows that of the all-sky dust forcing (Fig 11), internal ocean processes conspire to shift the maximum (in magnitude) of the cooling to the northwest of the maximum (in magnitude) forcing by approximately 1000 km. Despite this, the spatial pattern of the *ΔSST* and all-sky forcing composites are well-correlated with an r-value of 0.8 in those regions where *ΔSST* values are less than -0.05.

A five year composite difference of ocean currents averaged over the top 100 m of the model show an anomalous cyclonic circulation that opposes the subtropical gyre (Fig 12). This anomalous circulation is the geostrophic adjustment to cool anomalies (Fig 11) that extend below the surface (discussed further in Section 3d) and includes a cross equatorial flow from the warm to the cool hemisphere near the Brazilian coast that is coincident with the NBC. The western segment of the circulation follows the path of the Gulf Stream and the Caribbean current southward to near 15°N, where the flow travel eastward and then northeastward following the NEC.

The magnitude of the anomalous current speed is small, less than 0.1 cm s^{-1} (Fig 12). However, except for the western boundary currents, the climatological current speeds in the region of the dust-forced circulations are also small, everywhere less than 3 cm s^{-1} and in many areas less than 1 cm s^{-1} (Fig. 6). Thus, in some places the magnitude of the dust-forced changes in the 100 m averaged currents represent a significant portion of the climatological currents. For example, in the region of 10°N-30°N and 25°W-45°W the magnitude of the five year composite differences are 5-50% of the climatological current speed. Therefore, it is plausible that anomalous dust cover plays a non-negligible role in shaping ocean circulation over the eastern sector of the tropical North Atlantic.

The northward branch of the anomalous cyclonic circulation (Fig 12) is advecting warm water northward by acting on the positive meridional SST gradient (Fig 3), and thus may explain why the cooling maximum is offset to the northwest of the forcing maximum (Fig 11). Similarly, the southward branch of the anomalous circulation that overlays the gulf stream is advecting cool water equatorward, possibly explaining the cooler temperatures that lie to the northwest of the -1 W m^{-2} forcing contour. Relevance of advection to temperature anomalies in the 10°-20°N latitude is consistent with prior surface heat budget analysis (Foltz and McPhadden, 2006).

The relationship between circulation anomalies and dust-forced changes to the temperature of the upper ocean is elucidated by plotting composite streamline contours over composite upper ocean heat content (UOHC), defined as the ocean heat content integrated over the top 100 m of the model (Fig 13). The streamline contours generally follow the UOHC contours, and the spacing of the contours are closest where the UOHC

values are the largest in magnitude, suggesting that the circulation is a response to steric changes caused by the cool anomaly.

Composite differences of UOHC better match the pattern of dust-forced circulations integrated over the same depth than does the SST response alone (Fig 13). The maximum difference in UOHC composites is over -20 kJ cm^{-2}, centered on 30°W and 20°N. The contours of UOHC stretch southwestward from this maximum, following the anomalous currents, such that anomalies are greater (in magnitude) than -10 kJ cm^{-2} out to 50°W and 15°N. The -5 kJ cm^{-2} contour extends northward from the western boundary to 35°N, and the -0.2 kJ cm^{-2} contour nearly reaches the 45°N latitude. The UOHC contours cross those for ΔSST, suggesting that internal processes are shaping the response of the subsurface and are not only directly forced by changes to the surface heat flux (Fig 13). We also examined nortward volume transport integrated across 20°N in the model output. The northward transport varied in phase with the dust anomalies, although the magnitude of the anomalies were an order of magnitude smaller than observed decadal variability; anomalies O(-0.02) Sv during periods when dust is low (e.g., 1950s, 2000s), and O(0.025) during the peak in dustiness of the 1980s (not shown).

d. Evolution of subsurface temperature anomalies

Time series and composite differences of SST, upper ocean currents, and UOHC all suggest that Atlantic dust cover variability alters the physical structure of the tropical North Atlantic on interannual to possibly multidecadal time scales. It is therefore constructive to also consider the time evolution of dust-forced temperature anomalies at depth. Transects of dust-forces changes in potential temperature along an Atlantic transect at 20°N during 1984 (made by differencing the control from perturbation run, $\Delta\theta$)

provides insight into the mechanisms by which dust variability affects the subsurface and the $\Delta\theta$ anomalies are incorporated into the permanent thermocline (Fig 14).

During 1983 anomalously strong and persistent dust activity forced SST cool anomalies over the tropical northern Atlantic (Fig 8). As the winter mixed layer deepened in January 1984, cool anomalies were mixed down to the base of the mixed layer, a depth of 60-70 m (Fig 15). As the mixed layer begins to shoal in March 1984 the cool anomalies mixed down during the wintertime remain at depth. In May 1984 the mixed layer is near the minimum and summertime forcing by anomalously high dust cover begins to further cool the temperature of the mixed layer. As the mixed layer remains shallow throughout July, when the magnitude of dust-forced SST anomalies are at a maximum, mixed layer cool anomalies are O(0.5°C) along the eastern half of the transect, and appear to be mixing down below the base of the mixed layer. In September 1984 the magnitude of the SST anomaly is weakened, but the anomalies at depth are little changed. Finally, in November, as the mixed layer began to seasonally deepen the surface anomalies are also mixed down. Interestingly, in the November 1984 transect, temperature anomalies that had precipitated below the base of the mixed layer during the previous summer's months are of a magnitude greater than that of the mixed layer at 30°W, such that potential temperature anomalies actually increase with depth down to 40 m.

4. Discussion and Conclusions

Using a 54-year climatology of historical dust surface radiative forcing and an ocean general circulation model we estimated the physical response of the tropical North

Atlantic to anomalous African dust on decadal time scales. Based on the model output we found that the range of dust forced changes to tropical North Atlantic SST are *O*(0.5° C) across a broad region of 20°-45°W and 10-30°N (Fig 7). Over time the magnitude of the basin-averaged response varies on interannual to decadal time scales (Figs 8, 9), and on multidecadal time scales periods of warm and cool dust forced SST anomalies are in phase with -and of a magnitude comparable to- the AMO (Fig 9). Periods of dust-forced cool (warm) anomalies impose anomalous cyclonic (anti-cyclonic) circulation, and although the magnitude of the anomalous circulation was small, the change relative to the climatological currents was 1-25% (Figs 12, 13). In addition, during periods of strongly anomalous dust, the depth of the dust-forced temperature changes extended well below the base of the seasonal mixed layer, to depths of 125 m (Figs 14, 15).

In *Mahowald et al.* (2010) a composite map of the dust forced change in SST , similar to that in Figure 11 here except for 10-year composite differences, shows a region of cool anomalies ranging from 0.1°-0.5°C extending southwestward from 15°N and 15°W. A 10-year SST composite difference based on our data shows cool anomalies within this same range, although the anomalies mostly extend westward from 15°N (not shown). In *Mahowald et al.* (2010) dust-forced changes to SST are estimated using an atmospheric general circulation model coupled to a slab ocean, thus the similarity between their and our results suggest that to first order the aerosol direct effect is the primary mechanism for aerosol-forced SST variability, and that coupled effects and dynamic ocean processes may be neglected. However, such an assumption may not hold on longer time scales.

African dust outbreaks are thought to be modulated by periods of drought in the Sahel region of West Africa (*Prospero and Lamb* 2003), and there is a strong influence of tropical SST on West African rainfall on decadal time scales (*Giannini et al.* 2003). Given that dust forced SST anomalies are in-phase with observed SST anomalies and the AMO (Fig 9) it is plausible that a coupled relationship between surface, atmospheric, and oceanic processes governs regional climate behavior. Given the disagreement in dust fluxes in climate models (*Huneeus et al.* 2010; *Kok* 2011), and uncertainty in future changes to source regions with global warming (*Mahowald* 2007), we suggest that quantifying the processes governing dust variability, and the historical role of dust in shaping climate variability, is of paramount importance to estimating future change.

5. Acknowledgements

Funding for this work was provided by NOAA/CPO (NA10OAR4310136) to the University of Virginia.

6. References

Boyer, T. P., S. Levitus, H. E. Garcia, R. A. Locamini, C. Stephens, and J. Antonov (2005), Objective analyses of annual, seasonal, and monthly temperature and salinity for the world ocean on a 0.25 degrees grid, *Int. J. Climatol.*, **25(7)**, 931–945, doi:10.1002/joc.1173.

Deser, C., M. A. Alexander, and M. S. Timlin, 2003: Understanding the persistence of sea surface temperature anomalies in midlatitudes. *J. Climate*, **16**, 57–72.

Engelstaedter, S., I. Tegen, and R. Washington, 2006: North African dust emissions and transport. Earth-Sci. Rev., 79, 73-100.

Evan, A. T., A. K. Heidinger, R. Bennartz, V. Bennington, N. M. Mahowald, H. Corrada-Bravo, C. S. Velden, G. Myhre, and J. P. Kossin (2008), Ocean temperature forcing by aerosols across the Atlantic tropical cyclone development region, *Geochem. Geophys. Geosyst.*, **9**, Q05V04, doi:10.1029/ 2007GC001774.

Evan, A. T., D. J. Vimont, A. K. Heidinger, J. P. Kossin, R. Bennartz. (2009) The Role of Aerosols in the Evolution of Tropical North Atlantic Ocean Temperature Anomalies. *Science* **324**:5928, 778-781

Evan, Amato T., Sujoy Mukhopadhyay, 2010: African Dust over the Northern Tropical Atlantic: 1955–2008. *J. Appl. Meteor. Climatol.*, **49**, 2213–2229. doi: 10.1175/2010JAMC2485.1

Foltz, G.R., and M.J. McPhaden, 2006: The role of oceanic heat advection in the evolution of tropical North and South Atlantic SST anomalies. *J. Climate*, **19**, 6122-6138.

Foltz, G.R., and M.J. McPhaden, 2008a: Impact of Saharan dust on tropical North Atlantic SST. *J. Climate*, **21**, 5048-5060.

Foltz, G.R., and M.J. McPhaden, 2008b: Trends in Saharan dust and tropical Atlantic climate during 1980-2006. *Geophys. Res. Lett.*, **35**, L20706, doi:10.1029/2008GL035042.

Gent, P. R., and J. C. McWilliams (1990), Isopycnal mixing in ocean circulation models, *J. Phys. Oceanogr.*, **20**, 150 – 155, doi:10.1175/1520 0485(1990)020<0150:IMIOCM>2.0.CO;2.

Giannini, A., R. Saravanan, and P. Chang (2003), Oceanic forcing of Sahel rainfall on interannual to interdecadal time scales, *Science*, **302**, 1027– 1030.

Goldenberg, S. B., C. W. Landsea, A. M. Mestaz-Nunez, and W. M. Gray, 2001: The recent increase in Atlantic hurricane activity: Causes and implications. *Science*, **293**, 474–479.

Husar, R. B., J. M. Prospero, and L. L. Stowe (1997), Characterization of tropospheric aerosols over the oceans with the NOAA advanced very high resolution radiometer optical thickness operational product, *J. Geophys. Res.*, **102**(D14), 16,889–16,910, doi:10.1029/96JD04009.

Huneeus, N., et al. (2010), Global dust model intercomparison in AeroCom phase I, Atmos. Chem. Phys. Discuss., 10, 23,781–23,864, doi:10.5194/acpd-10-23781-2010

Kalnay, E., et al. (1996), The NCEP/NCAR 40-Year Reanalysis Project, *Bull. Am. Meteorol. Soc.*, **77(3)**, 437–471, doi:10.1175/1520-0477(1996) 077<0437:TNYRP>2.0.CO;2.

Kaufman, Y. J., I. Koren, L. A. Remer, D. Tanr, P. Ginoux, and S. Fan (2005), Dust transport and deposition observed from the Terra-Moderate Resolution Imaging

Spectroradiometer (MODIS) spacecraft over the Atlantic Ocean, *J. Geophys. Res.*, **110**, D10S12, doi:10.1029/2003JD004436.

Kok, J.F. (2011), A scaling theory for the size distribution of emitted dust aerosols suggests climate models underestimate the size of the global dust cycle, Proceedings of the National Academy of Sciences (PNAS), 108(3), 1016-1021,

Large, W. G., J. C. McWilliams, and S. C. Doney (1994), Oceanic vertical mixing: A review and a model with a nonlocal boundary layer parame- terization, *Rev. Geophys.*, **32**, 363–403, doi:10.1029/94RG01872.

Mahowald, N. M. (2007), Anthropocene changes in desert area: Sensitivity to climate model predictions, Geophys. Res. Lett., 34, L18817, doi:10.1029/2007GL030472.

Mahowald, N. M., et. al. Observed 20th century desert dust variability: impact on climate and biogeochemistry, *Atmos. Chem. Phys.*, **10**, 10875-10893, doi:10.5194/acp-10-10875-2010, 2010.

Marshall, J., A. Adcroft, C. Hill, L. Perelman, and C. Heisey (1997a), A finite volume, incompressible Navier-Stokes model for studies of the ocean on parallel computers, *J. Geophys. Res.*, **102**, doi:10.1029/96JC02775.

Marshall, J., C. Hill, L. Perelman, and A. Adcroft (1997b), Hydrostatic, quasi hydrostatic, and nonhydrostatic ocean modeling, *J. Geophys. Res.*, **102**, 5733–5752, doi:10.1029/96JC02776.

Martínez Avellaneda, N., N. Serra, P. J. Minnett, and D. Stammer (2010), Response of the eastern subtropical Atlantic SST to Saharan dust: A modeling and observational study, *J. Geophys. Res.*, **115**, C08015, doi:10.1029/2009JC005692.

Miller, R. L., and I. Tegen, 1998: Climate response to soil dust aerosols. J Clim, 11, 3247-3267.

Myhre, G., A. Grini, J. M. Haywood, F. Stordal, B. Chatenet, D. Tanre´, J. K. Sundet, and I. S. A. Isaksen (2003), Modeling the radiative impact of mineral dust during the Saharan Dust Experiment (SHADE) campaign, *J. Geophys. Res.*, **108**(D18), 8579, doi:10.1029/2002JD002566.

Prospero, J. M., and P. J. Lamb (2003), African droughts and dust transport to the Caribbean: Climate change implications, *Science*, **302**, 1024–1027.

Rayner, N. A., P. Brohan, D. E. Parker, C. K. Folland, J. J. Kennedy, M. Vanicek, T. J. Ansell, S. F. B. Tett, 2006: Improved Analyses of Changes and Uncertainties in Sea Surface Temperature Measured In Situ since the Mid-Nineteenth Century: The HadSST2 Dataset. *J. Climate*, **19**, 446–469. doi: 10.1175/JCLI3637.1

Santer, B., T. Wigley, C. Doutriaux, J. Boyle, J. Hansen, P. Jones, G. Meehl, E. Roeckner, S. Sengupta, and K. Taylor (2001), Accounting for the effects of volcanoes and ENSO in comparisons of modeled and observed temperature trends, *J. Geophys. Res.*, **106**(D22), 28033-28059.

Schollaert, S. E., and J. T. Merrill (1998), Cooler sea surface west of the Sahara Desert correlated to dust events, *Geophys. Res. Lett.*, **25**, 3529–3532.

Trenberth, K. E., and D. J. Shea (2006), Atlantic hurricanes and natural variability in 2005, *Geophys. Res. Lett.*, **33**, L12704, doi:10.1029/2006GL026894.

Wong, S., A. E. Dessler, N. M. Mahowald, P. R. Colarco, and A. da Silva (2008), Long-term variability in Saharan dust transport and its link to North Atlantic sea surface temperature, *Geophys. Res. Lett.*, **35**, doi:10.1029/2007GL032297.

Wong, S., A. E. Dessler, N. M. Mahowald, P. Yang, and Q. Feng (2009), Maintenance of lower tropospheric temperature inversion in the Saharan Air Layer by dust and dry anomaly, *J. Clim.*, **22**, 5149-5162.

Yoshioka, M., N. M. Mahowald, A. J. Conley, W. D. Collins, D. W. Fillmore, C. S. Zender, and D. B. Coleman, 2008: Impact of desert dust radiative forcing on Sahel precipitation: Relative importance of dust compared to sea surface temperature variations, vegetation changes, and greenhouse gas warming. J. Clim., 20, 1445-1467.

7. Figures

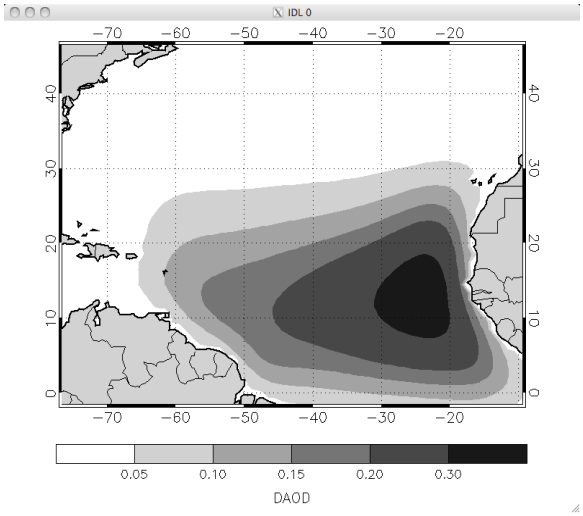

Figure 1. Long-term mean dust optical depth over the northern tropical Atlantic. Climatology is based on monthly mean values for the period 1955–2008, that were created with a statistical model to blend recent satellite observations with historical dust proxy data (cf. Evan and Mukhopadhyay 2010). Figure reproduced from AMS. Something about rivers!

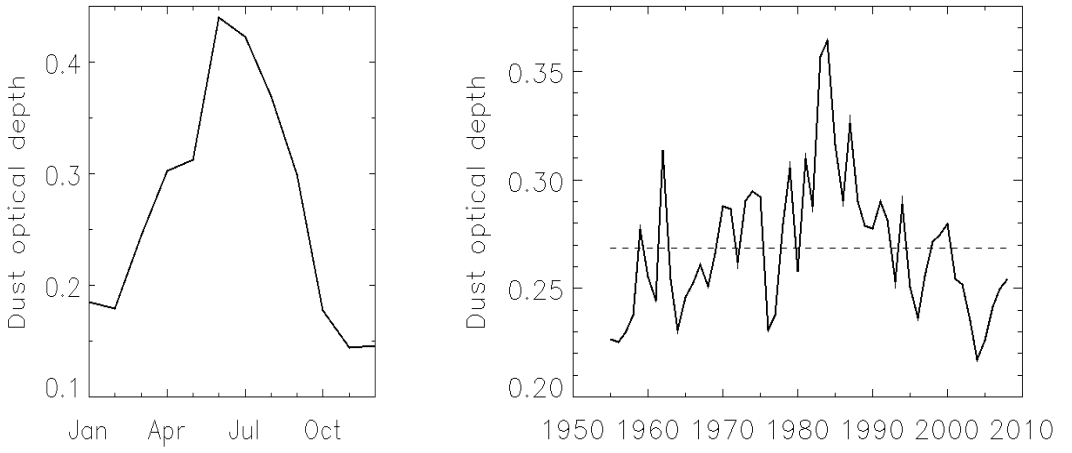

Figure 2. Seasonal cycle and annual mean time series of dust optical depth over the tropical northern Atlantic. Monthly climatological (left) and annual (right) average values are based on means from the 1955–2008 time period and are averaged over the region 10°-20°N and 20°-50°W. The maximum in dust cover occurs in June-July, and the minimum in November-December. See Evan and Mukhopadhyay (2010) for a detailed description of the data.

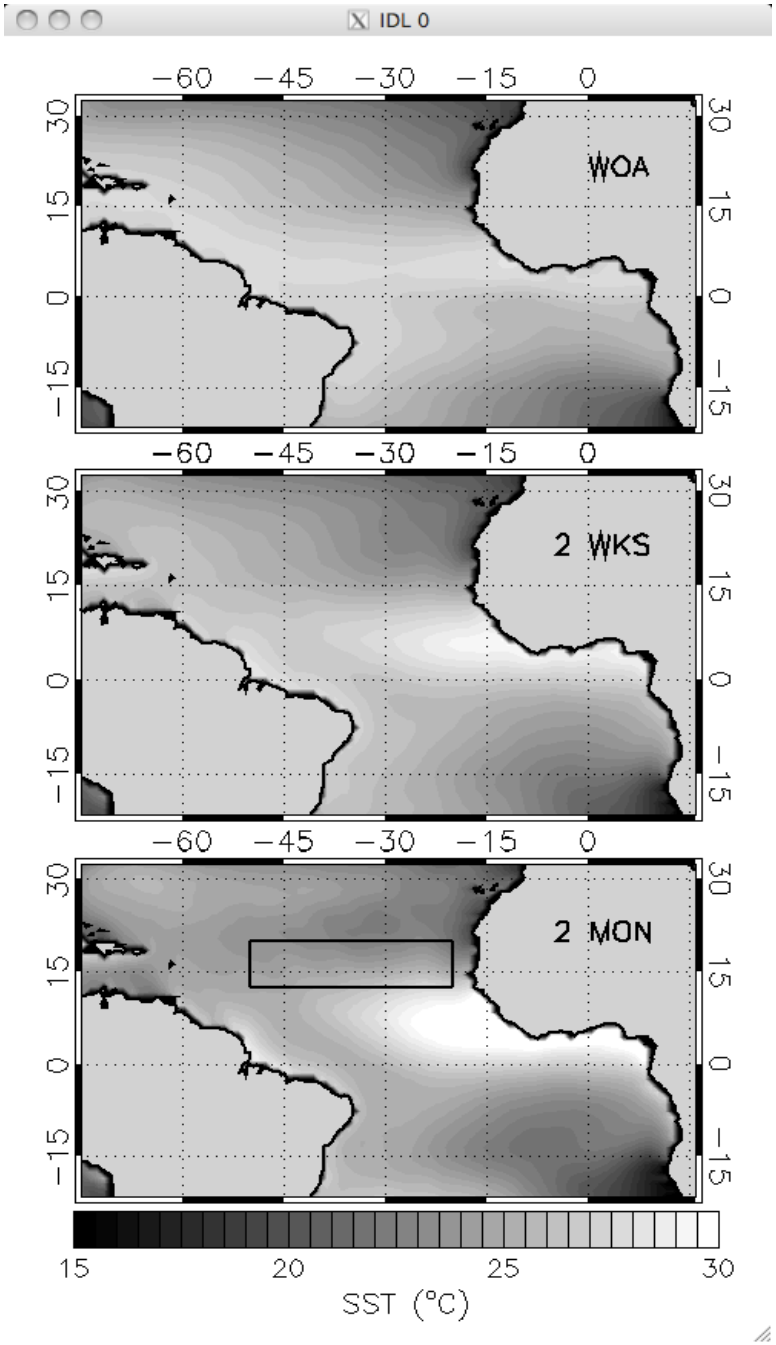

Figure 3. Difference between model output and observations of annual mean SST. Shown is the difference between annual average SST from output of the MITgcm and from the WOA05 climatology for model t_{relax} equal to two months (top) or two weeks (bottom). Model SST is based on the average from the last year of a 130 year model spinup. By design the model setup with a shorter relaxation time better reproduces the observed SST climatology, and in our region of study SST errors from t_{relax} of two months are less than $2°C$. The box outlined in the bottom panel indicates the region over which time series analysis is performed.

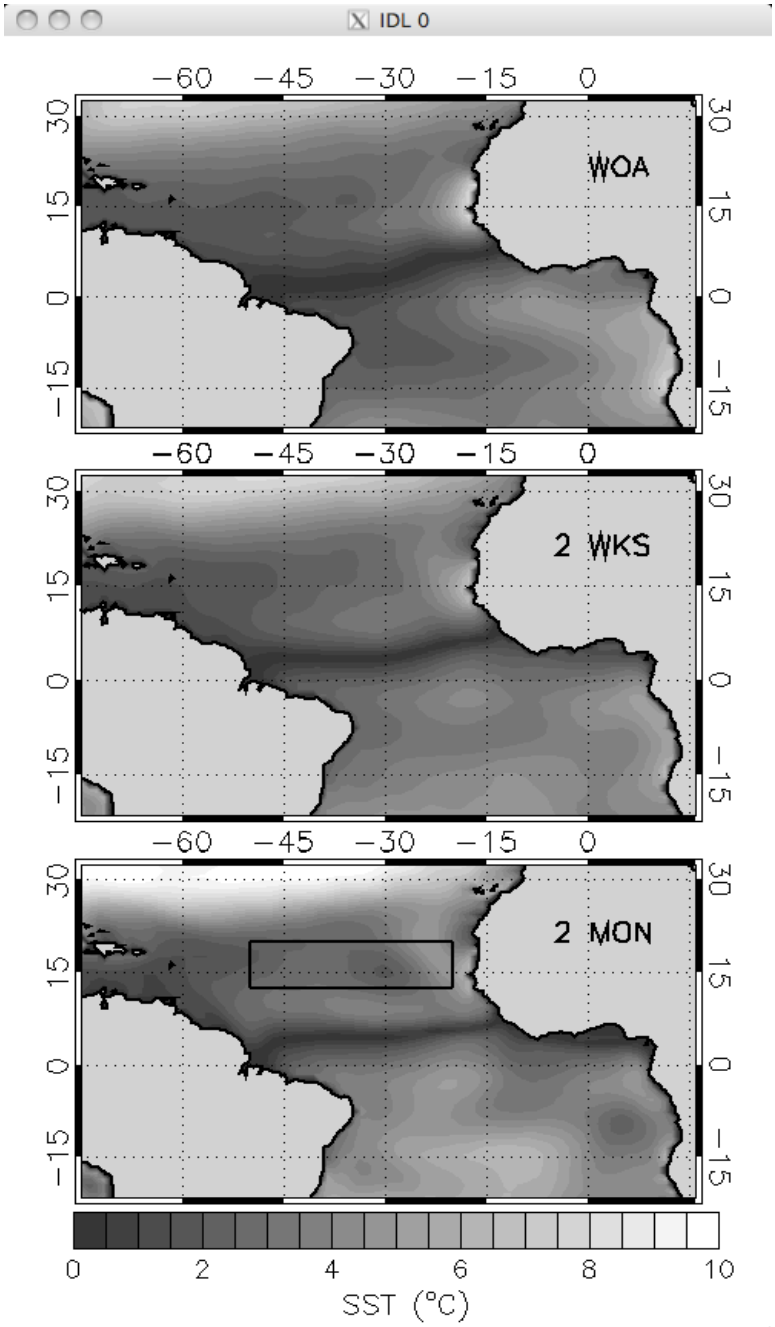

1

Figure 4. Difference between model output and observations in magnitude of the annual cycle. Shown is the difference between mean summer (JAS) and Winter (FMA) SST from MITgcm output and WOA05 climatology for model t_{relax} set to either two months (top) or two weeks (bottom). Model SST is based on the last year of a 130 year model spinup. Both model setups overestimate the magnitude of the seasonal cycle in the midlatitudes by greater than 1°C. In our region of interest the model overestimates and underestimates the magnitude of the seasonal cycle O(1°C) or less when t_{relax} equals two months. The box outlined in the bottom panel indicates the region over which time series analysis is performed.

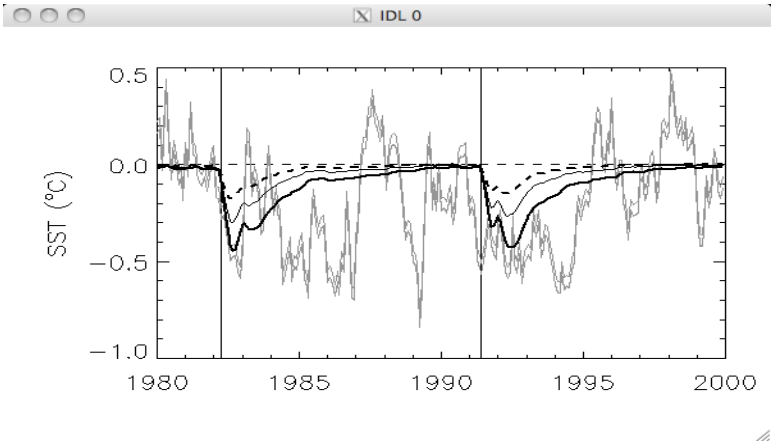

Figure 5. Observed and modeled SST changes following the eruptions of El Chichón (1982) and Mount Pinatubo (1991). Shown are time series of SST from the HADISST2 data set over the period 1980-2000 and averaged over the region 0°-30°N and 20°-65°W (gray lines). The spread of SST observations results from differences in the averaging time period used to calculate the mean from which deviations are plotted (one, two, and three years preceding the eruption of El Chichón), and vertical lines represent the time of each eruption. The time series in black (thick, thin, and dashed) represent the modeled response to each eruption over the same region, where the thick, thin, and dashed time series represent t_{relax} values of two months, one month, and two weeks, respectively. A larger value of t_{relax} tends to better match the observed response to each eruption.

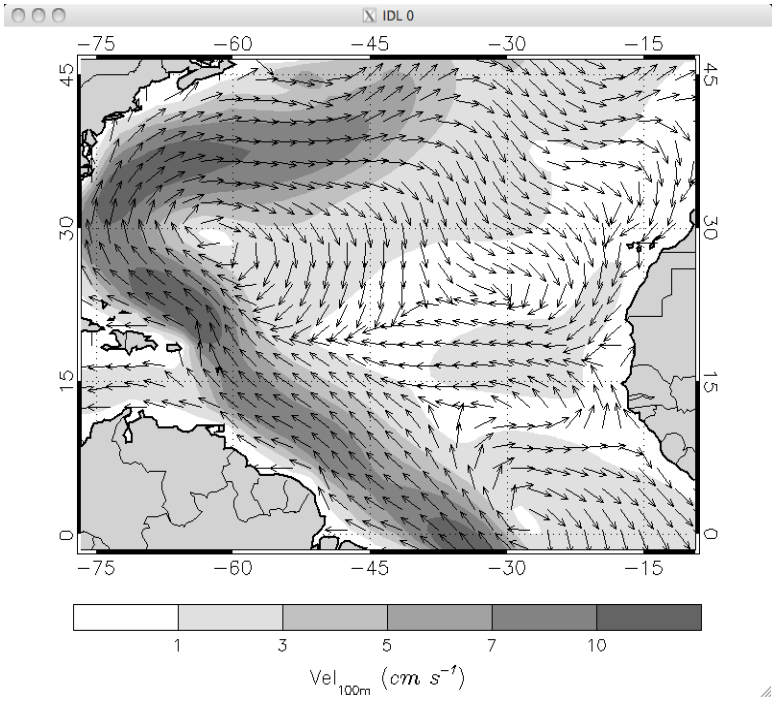

Figure 6. Annual model mean current direction and magnitude averaged over the top 100m. Annually averaged model velocity are from a single year climatology run following the 130 year spinup for t_{relax} of two months. Current magnitude is shaded from 1 $cm\ s^{-1}$ and direction is indicated by vectors of arbitrary length. The model is able to reproduce the major upper ocean currents of the equatorial and subtropical northern Atlantic.

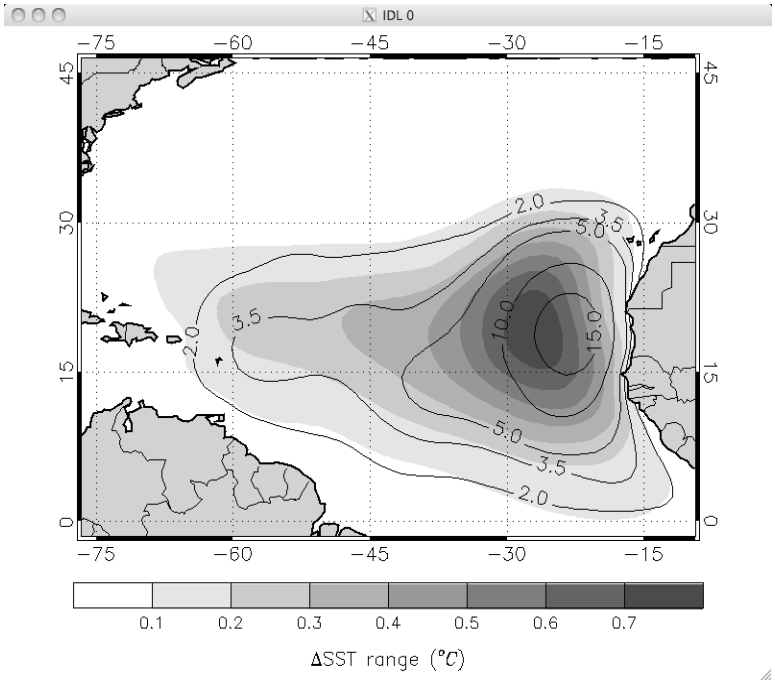

Figure 7. Range of dust-forced changes to northern tropical Atlantic SST and dust surface forcing over the period 1955–2008. As we only consider the effect of *anomalous* dust variability on ocean temperatures, the mean dust surface forcing from radiative transfer model output, and the mean effect of dust on surface temperatures, which is estimated by differencing control and perturbation model runs, are zero. A map of the range of dust-forced SST changes (shaded contours) from 0.1°C is used to indicate regions sensitive to mineral aerosol variability and the gray contours indicate the range of all-sky dust surface forcing ($W\ m^{-2}$). The black box encompasses the area 12.5°-25°N and 20°-50°W and is the region over which subsequent time series analysis is performed.

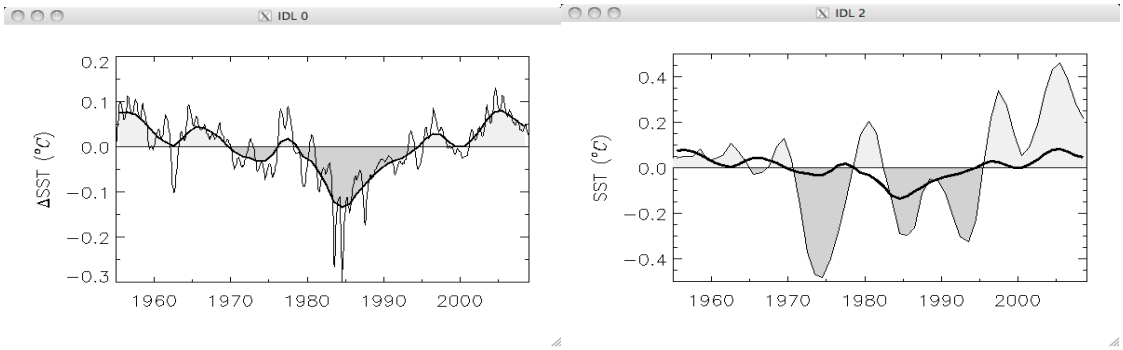

Figure 8. Annual mean time series of *ΔSST* and observed SST for 1955–2008. Monthly mean values are averaged over the region 12.5°-20°N and 20°-50°W (black contour, Fig 9). The shaded areas represent warm (red) and cool (blue) annual mean *ΔSST* (left) and observed SST (right) from the Hadley Centre, and both have been smooth with a 5 year low pass filter. The thin black line in the *ΔSST* series plot (left) is monthly mean *ΔSST*, and the thick black line overlaying the SST time series (right) is the same 5-year low pass filtered annual *ΔSST* (left). Positive *ΔSST* during the late 1950s and mid-2000s and negative *ΔSST* during the mid 1980's have been separately noted in earlier studies.

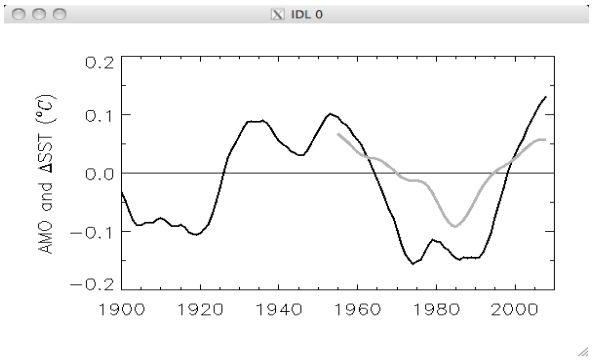

Figure 9. Time series of the AMO and smooth *ΔSST*. The AMO time series is constructed consistent with Trenberth and Shea (2006) and the *ΔSST* series is the annual time series shown in Figure 8 but also smoothed with a 13-point triangle filter (half-power at 15 years). Over the 54 years for which both data are available the low frequency *ΔSST* variability is in phase with the AMO.

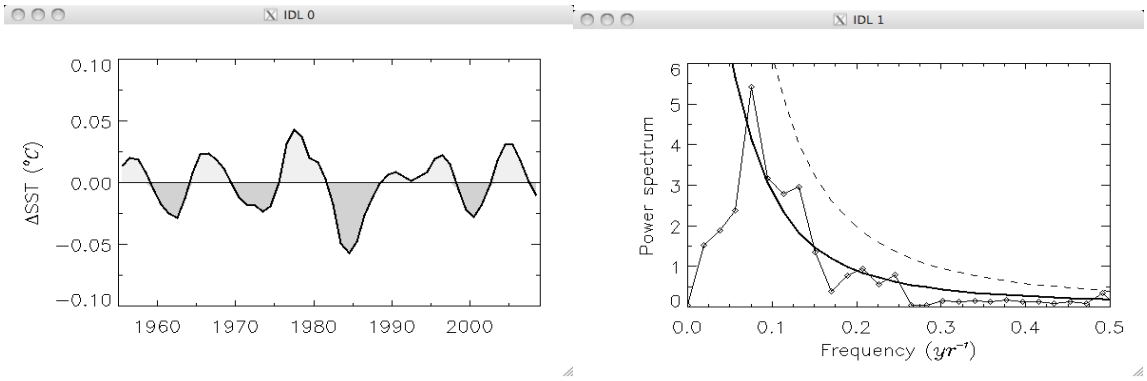

Figure 10. Band pass filtered annual mean time series of *ΔSST* for 1955–2008 and FFT. Time series of *ΔSST* (left) averaged over the region 12.5°-20°N and 20°-50°W (black contour, Fig 9). The *ΔSST* time series is smoothed with a 5-year low pass filter and a 20-year high pass filter, with the endpoints retained, in order to highlight decadal variability. The power spectrum (right) is the FFT of the band-pass filtered *ΔSST* series and shows spectral peaks (thin black line) that are larger than an equivalent red noise spectrum (thick black line) at periods of 7–13 years. Note that none of the spectral peaks are statistically significant at the 95% level.

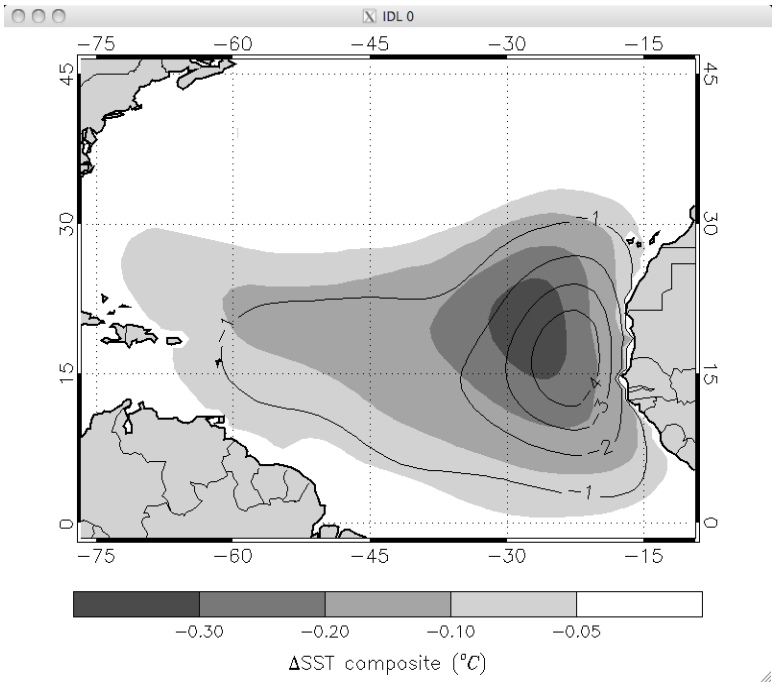

Figure 11. Composite maps of *ΔSST* and *ASF* for the difference between the five years of the largest negative and positive *ΔSST*. Composite differences of *ΔSST* (shading) and all-sky dust surface forcing (contours, Wm^{-2}), are defined as the annual means of the five years of minimum (1983–1988) minus maximum (1955–1957, 2004, 2005) *ΔSST* anomalies (Fig. 8). In the eastern half of the basin contours of *ΔSST* are displaced to the northwest of the forcing contours.

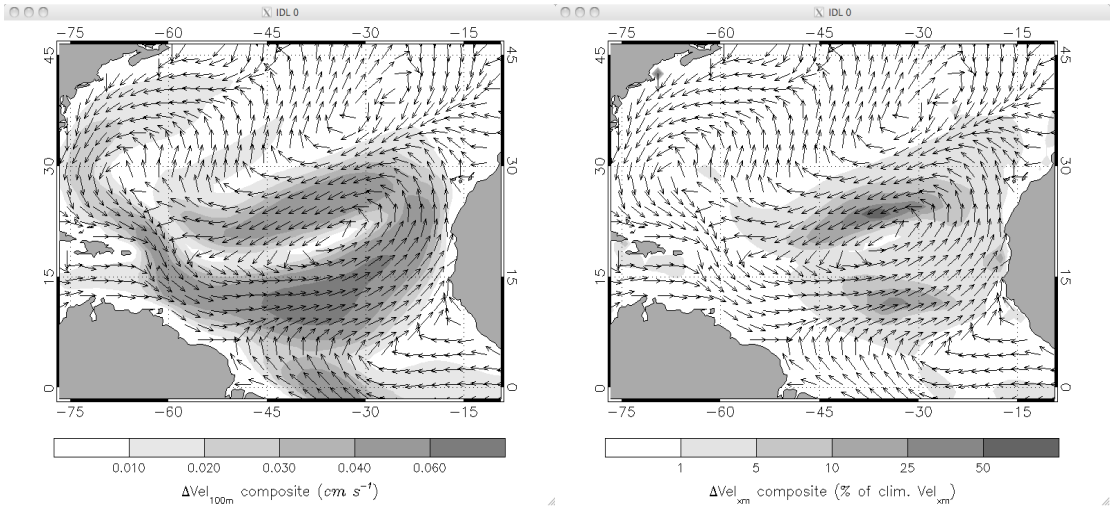

Figure 12. Composites of Vel_{100m} and Vel_{100m} as a fraction of the mean current magnitude. Contours are constructed in the same manner as described in Figure 11. Arrows are unit length and indicate direction of the anomalous current only. At left shading represents the magnitude of the circulation averaged over the upper 100 *m*. The magnitude of the anomalous circulation as a percent of the climatological (model) current magnitude, also averaged over the top 100 *m* of the model, indicates the relevance of the anomaly with respect to the mean state (right).

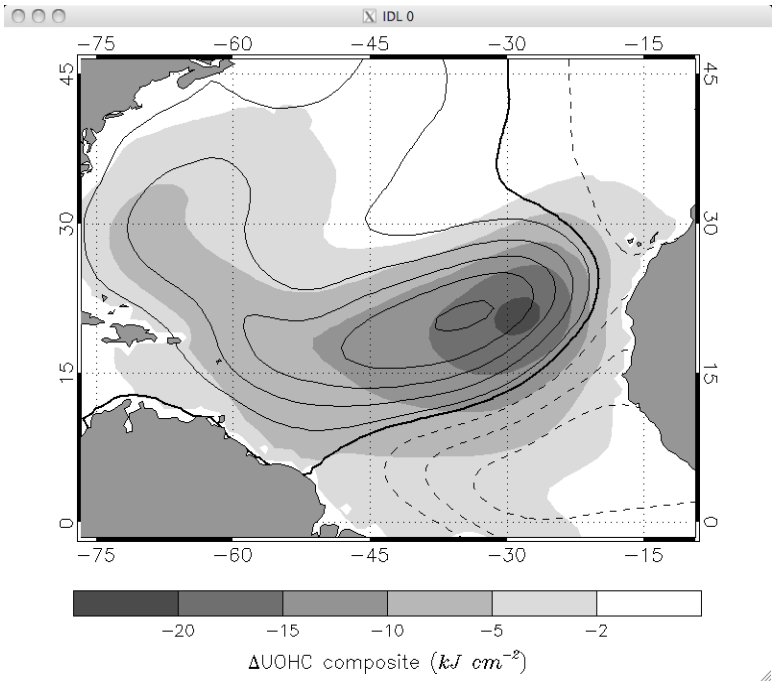

Figure 13. Streamfunction and *UOHC* composite map. Description of composites is the same as Figure 11. The streamfunction contours are from on the non-divergent part of the Vel_{100m} composites (Fig 12) and suggest anomalous circulations that govern the displacement of *UOHC* anomalies away from the region of direct surface forcing (Fig 11). Positive (negative) streamfunction contours indicate counterclockwise (clockwise) rotation, and the distance between contours indicate magnitude of the anomalous circulation.

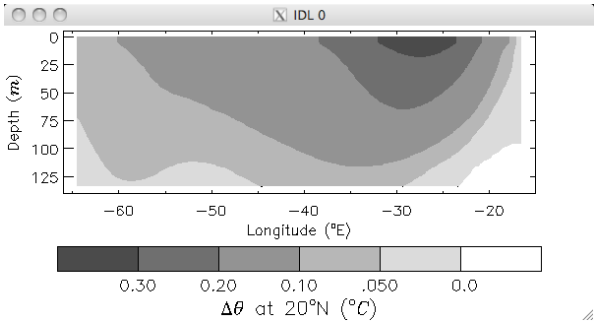

Figure 14. Composite of dust forced potential temperature along the 20°N transect. Composite description is the same as Figure 11. Potential temperature anomalies of $0.1°C$ extend to a depth of 100 m, and the longitude of the maximum depth of each

contour migrates westward with depth.

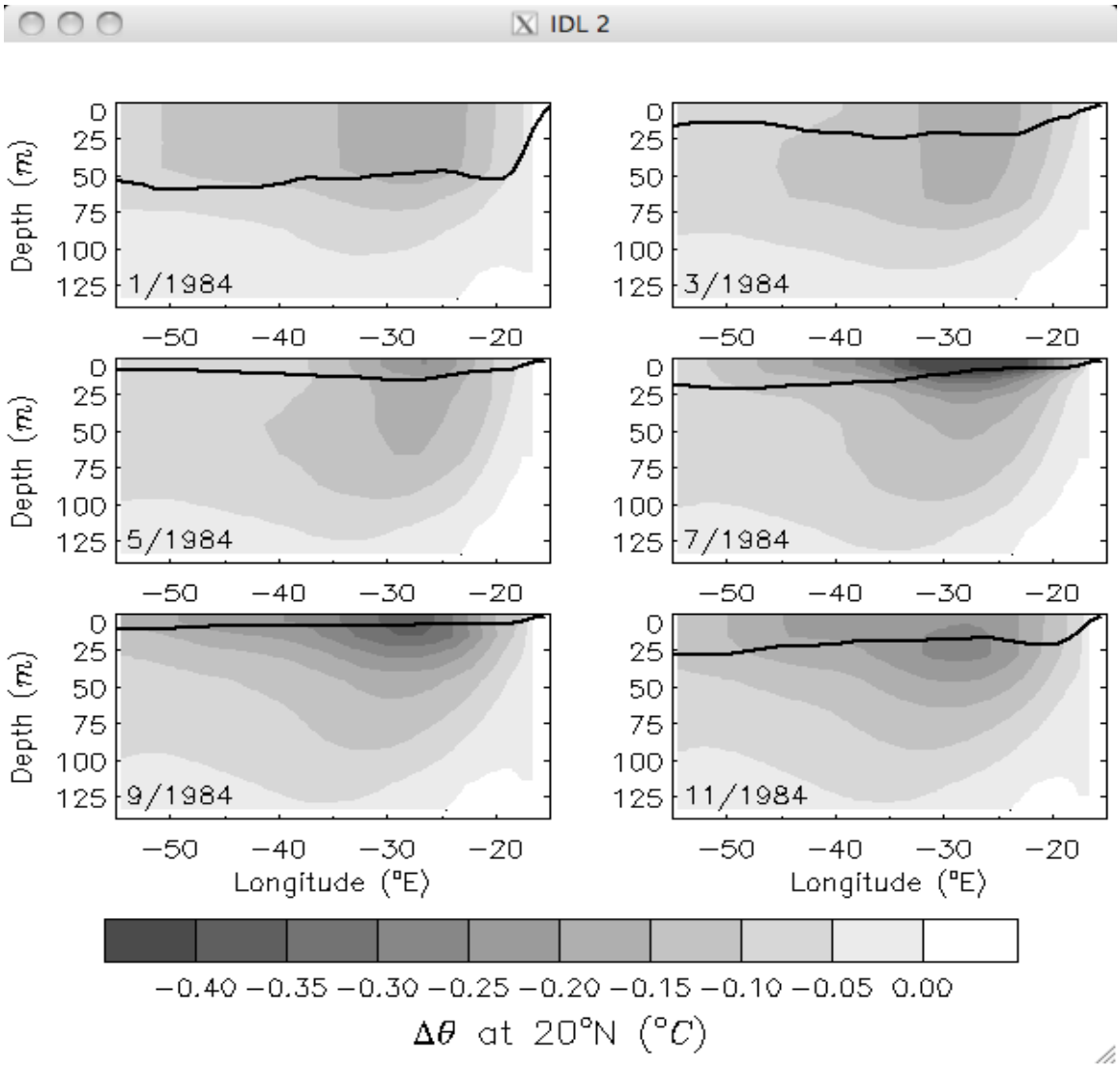

Figure 15. ΔT at depth along the 20°N transect during 1984. Shown are the monthly mean dust-forced change in potential temperature $\Delta\theta$ at depth (shaded contours) and the depth of the model mixed layer (interpolated) based on the 0.125σ criteria. Note that $\Delta\theta$ anomalies extend below the depth of the wintertime mixed layer, and are thus incorporated into the permanent thermocline.